Silicon Photonic Single-Segment IQ Modulator for Net 1 Tbps/λ Transmission Using All-Electronic Equalization

Essam Berikaa, *Graduate Student Member, IEEE*, Md Samiul Alam, *Graduate Student Member, IEEE*, Alireza Samani, Eslam El-Fiky, Yixiang Hu, Stéphane Lessard, and David V. Plant, *Fellow, IEEE*

(Post-Deadline Paper)

***Abstract*—There is a continuous need to scale optical communication networks' capacity to cope with the exponential growth of data traffic. Silicon photonics (SiP) retains significant potential as a platform for optical transceivers due to its CMOS compatibility, despite its limited electro-optic bandwidth and high driving voltage requirements. Here we present the design and characterization of two single-segment C-band SiP in-phase quadrature modulators (IQM) that differ in the phase shifter length, and we analyze the design tradeoffs based on their transmission performance. The large-signal transmission experiments indicate that the long IQM supports higher data transmission rates, which has 36 GHz 6-dB bandwidth and 10.5 V DC V_π under 1 V reverse bias. With all-electronic equalization and on a single polarization, we transmit net 413 Gbps (95 Gbaud 32QAM) over 80 km of standard single-mode fiber (SSMF) under the 14.8% overhead concatenated forward error correction (C-FEC) BER threshold of 1.25×10^{-2}. Using dual-polarization (DP) emulation and lookup table-based nonlinear pre-distortion (NLPD), we demonstrate the transmission of 95 Gbaud DP-32QAM and 115 Gbaud DP-16QAM over 80 km of SSMF below the C-FEC BER threshold, corresponding to net rates of 827 Gbps and 800 Gbps, respectively. Moreover, we transmit 105 Gbaud DP-64QAM over 80 km below the 25% overhead soft-decision (SD) FEC BER threshold of 5×10^{-2}; featuring the first demonstration of net 1 Tbps transmission using an all-silicon IQM. Employing only electronic equalization and single-segment IQM preserves the conventional architecture of coherent networks and transceivers, and highlights the potential of SiP as a platform for next-generation 800G applications.**

***Index Terms*—All-silicon IQ modulator, high symbol rate transmission, optical fiber communication, silicon photonics.**

Manuscript received 30 May 2022; revised 29 June 2022; accepted 12 July 2022. Date of publication 14 July 2022; date of current version 16 February 2023. (*Corresponding author: Essam Berikaa.*)

Essam Berikaa, Md Samiul Alam, Alireza Samani, Yixiang Hu, and David V. Plant are with the Photonic Systems Group, Department of Electrical and Computer Engineering, McGill University, Montréal, QC H3A 0E9, Canada (e-mail: essam.berikaa@mail.mcgill.ca; md.samiul.alam@mail.mcgill.ca; alireza.samani@mail.mcgill.ca; yixiang.hu@mail.mcgill.ca; david.plant@mcgill.ca).

Eslam El-Fiky is with the Photonic Systems Group, Department of Electrical and Computer Engineering, McGill University, Montréal, QC H3A 0E9, Canada, and also with the Department of Electrical Engineering, Alexandria University, Alexandria 21544, Egypt (e-mail: eslam.elfiky@mail.mcgill.ca).

Stéphane Lessard is with the Ericsson Canada, Montréal, QC H4S 0B6, Canada (e-mail: stephane.lessard@ericsson.com).

Color versions of one or more figures in this article are available at https://doi.org/10.1109/JLT.2022.3191244.

Digital Object Identifier 10.1109/JLT.2022.3191244

I. Introduction

THE growing data traffic demand driven by the wide deployment of bandwidth-hungry applications, such as high-definition video streaming and artificial intelligence, is mandating the increase in optical communication networks' capacity. Therefore, the Optical Internetworking Forum (OIF) started defining the specifications of the next-generation 800G coherent optical communication interfaces [1]. Currently, 400ZR coherent interfaces are based on 60 Gbaud dual-polarization (DP) 16 quadrature amplitude modulation (QAM) format. However, realizing 800 Gbps using 16QAM requires operating at 120 Gbaud, which challenges the bandwidth the electro-optic components. Thus, 96 Gbaud DP-32QAM and probabilistically shaped (PS) 100 Gbaud DP-64QAM are potential candidates for the next-generation 800G networks as they relax the bandwidth requirements [2], [3]. Increasing the QAM order needs driving electronics with higher effective number of bits (ENOB) and higher driving swings, and PS adds considerable load on the application-specific integrated circuits (ASICs) power consumption. Therefore, these different candidate modulation formats are being researched extensively to address these tradeoffs.

The SiP platform has numerous advantages such as low fabrication costs, CMOS compatibility, high yield, and the small form factor. However, its deployment in next generation coherent optical communication networks is facing the platform challenges in terms of the relatively limited electro-optic bandwidth and the high driving voltage requirements. However, the continuous increase in the bandwidth of digital-to-analog converters (DAC) is progressively pushing the limits of what can be achieved using SiP modulators. Recent years have witnessed several high-speed demonstrations using SiP IQMs. The transmission of 100 Gbaud 32QAM at a bit error rate (BER) of 2.4×10^{-2} below the 20% overhead (OH) soft-decision forward error correction SD-FEC threshold on a single polarization using SiP IQM has been reported, corresponding to a net rate of 416 Gbps [4]. Using adaptive iterative non-linear pre-distortion, joint electrical-optical pre-compensation, and DP emulation, the authors successfully transmit 100 Gbaud DP-32QAM under the 2.4×10^{-2} SD-FEC threshold, which corresponds to a net rate of 833 Gbps [5], [6]. To realize higher-bandwidth operation, segmented electrode designs are employed instead of the

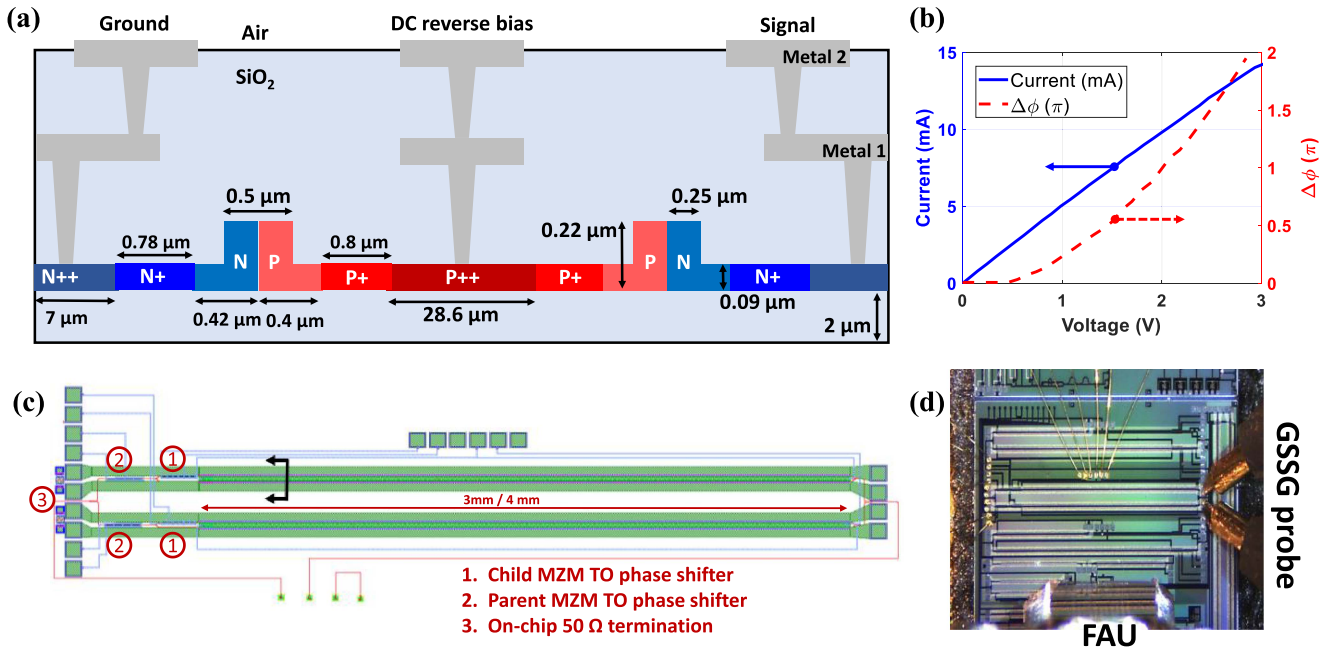

Fig. 1. Cross-sectional illustration of the child MZM structure (not to scale). (b) The IV and the phase-change ($\Delta\Phi$) versus voltage curves of the MZM's thermo-optic tuners. (c) The schematic of the IQM. (d) Top view of the wirebonded chip showing the position of the fiber array unit (FAU) and the RF probe.

conventional single-segment traveling-wave (TW) MZM electrodes as it reduces the microwave losses and improves the electro-optic bandwidth [7], [8]. In [9], a segmented-electrode IQM and joint electrical-optical pre-compensation have been used in transmitting 120 Gbaud 32QAM on a single polarization at back-to-back (B2B) under the 5×10^{-2} BER threshold of the 25% OH SD-FEC, corresponding to a net rate of 480 Gbps. However, the number of transmitter RF components scales with the number of electrode segments, which increases cost, power consumption, and packaging complexity. Besides, the optical pre-compensation requires optical filtering with waveshapers, band-pass filters, and additional EDFAs to compensate for their losses; which is impractical. Practically, single-segment IQMs and all-electronic pre-compensation are desired, as they do not alter or introduce extra overheads to the fiber-optic transmission network.

This paper presents the design and characterization of two SiP IQMs with different phase-shifter lengths. Both IQMs are tested in the C-band at B2B and after 80 km of SSMF. We examine the IQMs performance considering different QAM orders and at high symbol rates using a SiGe 128 GSa/s arbitrary waveform generator (AWG). Additionally, we highlight the design tradeoffs and analyze the difference in the performance of the two IQMs. Recently, we demonstrated the transmission of 105 Gbaud DP-64QAM using the longer IQM and all-electronic equalization over 80 km of SSMF under the 5×10^{-2} BER threshold of the 25% OH SD-FEC; featuring a record net rate of 1 Tbps (line rate of 1.26 Tbps) [10]. In this paper, we provide more insights into the experimental aspects of system optimization enabling the transmission of such ultra-high symbol rate signals despite the modest bandwidth of the SiP IQM, with a more in-depth characterization of the large-signal transmission performance.

The rest of this paper is structured as follows. Section II describes the modulator structure and presents the small-signal characterization of both IQMs. Section III describes the experimental setup and the digital signal processing (DSP) routine employed in the transmission experiment. The single polarization and dual-polarization transmission results along with the optical signal-to-noise ratio (OSNR) performance are given in Section IV and Section V concludes this work.

II. Modulators Design and Characterization

This section presents the design and characterization of the fabricated IQMs. The SiP modulators were fabricated through CMC Microsystem in a multi-project wafer (MPW) run at the Advanced Micro Foundry (AMF), which uses a conventional CMOS-compatible process flow. As depicted in Fig. 1(a), AMF's silicon-on-insulator (SOI) process employs a 220 nm thick silicon layer with 2 μm buried oxide. The IQM is composed of two parallelly connected child TW-MZMs. Each of the child MZMs requires a single RF signal; as it is a single segment MZM with the PN junctions designed for series push-pull (SPP) driving configuration [11]. The traveling-wave electrodes of each MZM are terminated with an on-chip 50 Ω termination (OCT) for maximum power transfer and ease of testing. The arms of the parent MZM are 305 μm apart, which minimizes the crosstalk between the I and Q quadratures. Both the child and parent MZMs are balanced, such that both arms of each MZM have the same length. Thus, the structure employs 4 thermo-optic (TO) heaters for biasing the IQM. The child MZMs' TO phase shifters set both MZMs at null and one of the parent TO phase shifters is used to induce 90^0 phase shift between the outputs of the child MZMs. The last TO phase shifter is left unbiased and only added to the design so that the propagation loss of the I and Q quadratures are matched [12].

As aforementioned, this work evaluates the performance of two IQMs that have the same structure but differ only in the phase shifter length and filling factor: 1) short IQM with 3 mm phase shifters at 90% fill factor, and 2) long IQM with 4 mm phase

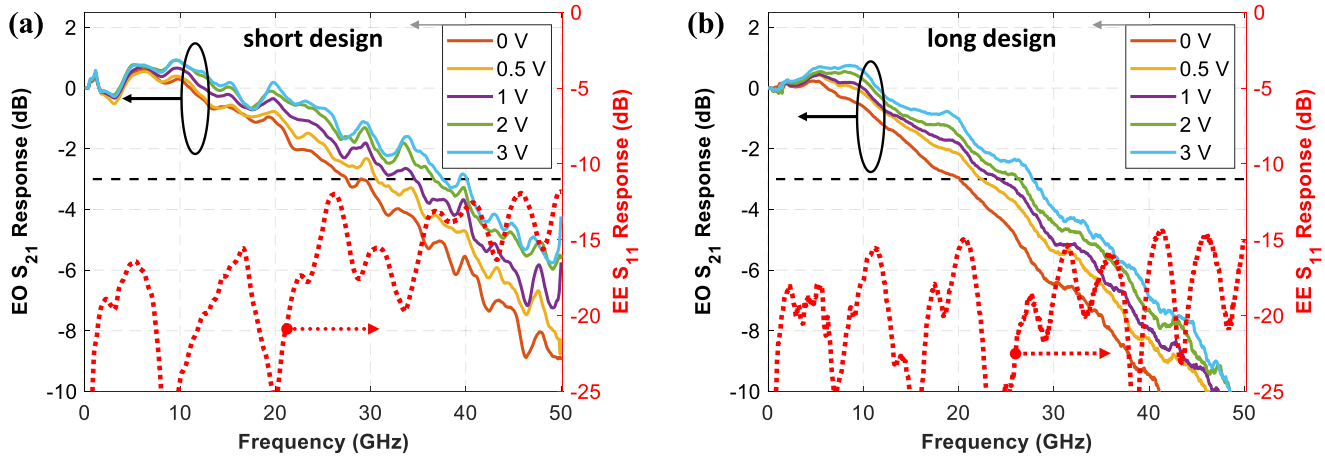

Fig. 2. The electro-optic S_{21} and electrical S_{11} (0 V) measurements for (a) the 3 mm (short) IQM and (b) the 4 mm (long) IQM.

shifters at 85% fill factor. The added undoped (intrinsic) sections reduce the effective phase shifter length; however, it prevents the flow of electric currents through the optical waveguides. The cross-sectional view of one of the child MZMs is depicted in Fig. 1(a). The rib waveguide width is 0.5 μm for nearly single-mode propagation across the C-band, and the width of the P, P+, P++, N, N+, and N++ regions are optimized through simulations to address the trade-off between minimizing the optical propagation loss and increasing the junction capacitance. The SPP configuration connects the two PN junctions in series, which halves the junction capacitance and increases the series resistance. The lower junction capacitance reduces the microwave losses and effectively improves the IQM bandwidth. The reverse DC bias is applied through a high-inductance line so that the RF and DC are separated. The complete design procedure of the employed TW-MZM coplanar strip electrodes is presented in [11]. The foundry process flow uses a 2 μm thick aluminum layer for metallization. As in [11], the width and separation between MZM electrodes are set to 36 μm and 60 μm, respectively. These values ensure that each of the electrodes has a 50 Ω characteristic impedance, besides ensuring a good velocity matching between the optical and RF signal. The OCTs are designed based on highly doped N++ silicon that results in 50 Ω resistances. The IQM layout and an image of the wire-bonded chip marking the position of the fiber array unit (FAU) and the RF GSSG probe are shown in Fig. 1(c)–(d). The employed TO phase shifter is described in [13], which is composed of parallelly connected resistors for power-efficient operation. These resistors are highly doped N++ silicon slabs surrounding the undoped optical rib waveguide. The measured IV characteristics and the phase-change ($\Delta\Phi$) versus voltage of one of the phase shifters are given in Fig. 1(b). The IV curve is not perfectly linear as its slope decreases at high voltage. The TO phase shifter requires 2 V to induce a π phase shift.

The measured DC V_π at 0 V reverse bias for the short and long designs are 12 V and 8.5 V, and the corresponding phase-shifting ($V_\pi L$) inverse efficiencies are 3.6 V.cm and 3.4 V.cm, respectively. The V_π of the IQMs can be almost halved if dual-drive IQM structure is adopted; however, it would require differential driving with four RF amplifiers. Alternatively, employing an L-shaped PN junction instead of the lateral junction can improve the phase-shifting efficiency and reduce the V_π. Fig. 2(a)–(b) show the small-signal response of both IQMs for one of the child MZMs. Fig. 2(a) shows that the short modulator has a 3-dB bandwidth of 27.5 GHz without reverse biasing and increases to 38 GHz at 3 V reverse bias, while the 6-dB bandwidth at 3 V is more than 50 GHz. Fig. 2(b) shows that the longer design has a lower 3-dB bandwidth of 20 GHz at 0 V reverse bias that reaches 28 GHz at 3 V. Both IQMs have a slow roll-off frequency response, which allows operating at high symbol rates as shown in the next sections. For both IQMs, the electrical S_{11} is below -10 dB up to 50 GHz; highlighting the good design of the traveling wave electrodes and the good impedance matching between the fabricated electrodes and the OCTs. Optically, the IQMs are connected to vertical grating couplers (GCs) for light coupling. The back-to-back coupling loss is 11 dB (5.5 dB/GC); employing edge couplers (1.5 dB/facet) can reduce the losses and lead to better transmission performance. Excluding GCs and routing losses, the measured insertion loss for the short and long IQMs is 3.5 dB and 4.5 dB, respectively.

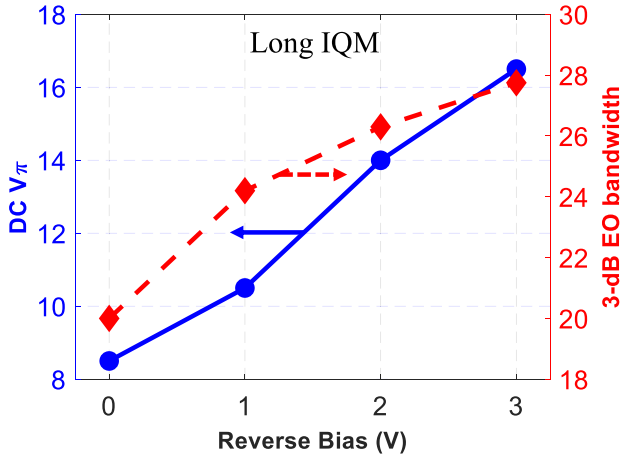

Fig. 3. Measured DC V_π and 3-dB EO bandwidth versus reverse bias voltage for the long IQM.

Increasing the IQM reverse bias decreases its optical propagation losses and increases its EO bandwidth; however, it increases its V_π resulting in higher modulation loss [14], [15]. The measured DC V_π and EO bandwidth at different reverse bias levels of the long IQM are shown in Fig. 3. There is a tradeoff

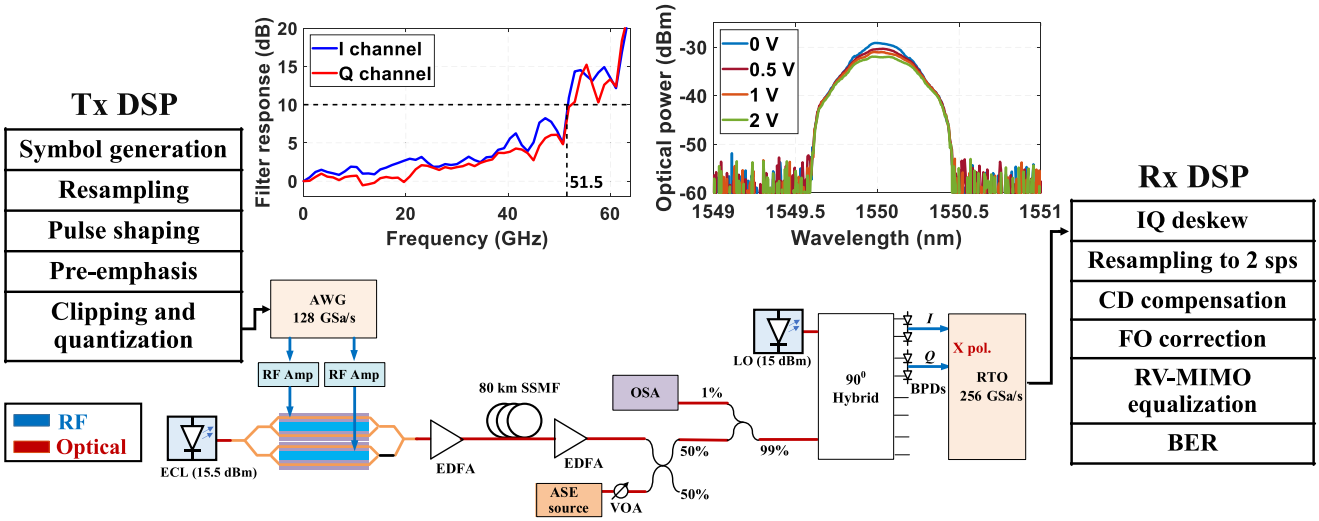

Fig. 4. The experimental setup and the DSP routine employed. The insets show the pre-compensation filter response for both I and Q channels (Left), and the optical spectra of 100 Gbaud 32QAM signals at different reverse bias levels using the long IQM at 0.05 nm resolution (Right).

between increasing IQM bandwidth and reducing its V_π. In our case, the performance is limited by the IQMs high V_π; thus, low reverse bias voltages yielded the optimum performance for both IQMs.

III. Experimental Setup and Digital Signal Processing

Fig. 4 shows the experimental setup and the DSP routine employed for testing the IQMs. At the transmitter, the desired QAM order symbols are created from a pseudorandom binary sequence (PRBS), which is then upsampled and pulse shaped using a root raised cosine (RRC) filter. The RRC filter roll-off factor is optimized for each symbol rate. The frequency response of the transmitter RF chain is pre-compensated using a digital filter for each quadrature which includes two AWG channels operating at 128 GSa/s and 26 dB gain 42-GHz RF amplifiers. The pre-compensation filters are given in the left inset of Fig. 4, the 10-dB point is around 51 GHz. We used higher swing from AWG for the I channel to match the SNR and driving voltage after the RF amplifier; which can be attributed to the slightly different frequency response of the RF amplifiers and the pre-compensation filters. The employed AWG has high output swing (up to 830 mVpp) with high signal fidelity, which enables pre-compensating 10 dB at the transmitter without degrading the signal quality. This unique feature and the precise pre-compensation of the frequency response of the transmitter RF chain alleviate all the bandwidth limitations in the system except for the SiP IQM, which is equalized at the receiver. Then, the amplified RF signals are loaded to the IQM using a 67 GHz GSSG probe. Optically, an external cavity laser (ECL) operating at 1550 nm with 15.5 dBm optical power and less than 100 kHz linewidth feeds the IQM. A tunable-gain EDFA is used to compensate for the GCs losses and boost the signal before the coherent receiver. Both IQMs are tested at B2B and after 80 km transmission. For the 80 km case, another EDFA is used to compensate for the 16 dB fiber loss. The transmitted signal is then coupled with an amplified spontaneous emission (ASE) noise signal using a 3-dB coupler. The ASE noise source is followed by a variable optical attenuator (VOA) to control the OSNR of the signal fed to the coherent receiver for OSNR sensitivity measurements. We used a 2×8 dual-polarization optical hybrid for both single and DP measurements. Another ECL operating at 1550 nm with 15 dBm power is used as a local oscillator (LO) laser; with effectively 12 dBm mixed with each polarization. The outputs of the optical hybrid are detected by 70 GHz balanced photodiodes (BPD) followed by a 256 GSa/s real-time oscilloscope (RTO) with a 64 GHz brick-wall filter. The received signals are then processed offline. At the receiver, Gram-Schmidt orthogonalization is used to compensate for the hybrid imperfections. Then, the signals are resampled to 2 samples per symbol (sps) for chromatic dispersion (CD) compensation and the frequency offset (FO) correction. A RRC matched filter is employed to maximize the SNR. For alleviating the linear distortion and phase noise, we employed a T/2-spaced 101-tap multiple-input-multiple-output (MIMO) equalizer with real-valued (RV) coefficients interleaved with a second order phase-locked loop (PLL) as described in [16]. A 2×2 MIMO equalizer is employed for single polarization transmission, while a 4×4 equalizer is used in the DP case for polarization tracking. The real-valued MIMO equalizer can correct the timing skews and power imbalance between the I and Q quadratures as it filters the signal quadratures independently, which is advantageous given that the employed BPDs are not matched. Eventually, the recovered symbols are demapped to bit sequence for BER calculation.

The inset of Fig. 4 shows the optical spectrum measured at 0.05 nm resolution of 100 Gbaud 32QAM signals using the long IQM at different reverse bias levels. The increase in reverse bias increases V_π and decreases the modulation depth ($V_{modulation}/2V_\pi$), leading to higher modulation loss and lower OSNR.

IV. Transmission Experiment Results

The performance of the short and long IQMs is investigated by transmitting different QAM orders at different symbol rates at B2B and 80 km of SSMF. The AWG output voltage, pulse shaping roll-off factor, and transmitter clipping ratio are optimized simultaneously at each symbol rate to achieve the lowest BER.

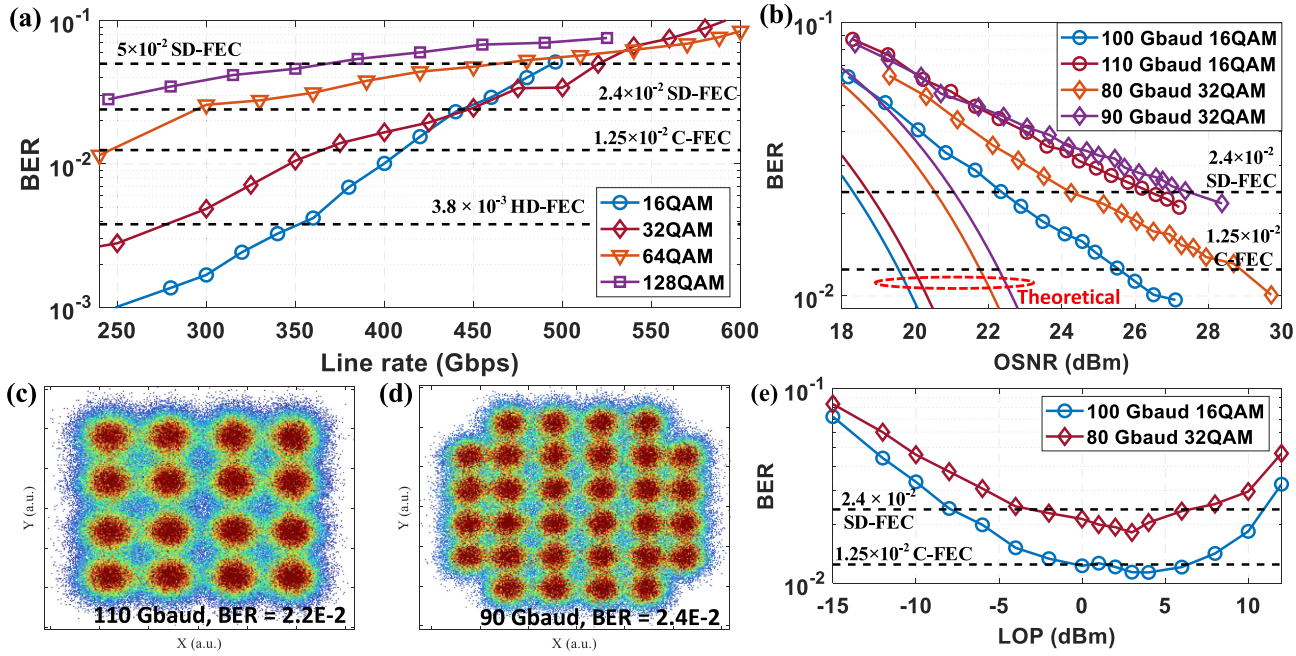

Fig. 5. (a) BER versus line rate for different QAM orders after 80 km transmission using the short IQM. (b) The OSNR performance at 0.1 nm. Recovered constellation for (c) 110 Gbaud 16QAM and (d) 90 Gbaud 32QAM. (e) BER versus LOP for 80 km transmission.

TABLE I
SUMMARY OF NET BITRATE ACHIEVED AFTER 80 KM TRANSMISSION ON A SINGLE POLARIZATION

BER threshold	FEC OH	Short (3 mm) IQM		Long (4 mm) IQM	
		Modulation format	Net bitrate (Gbps)	Modulation format	Net bitrate (Gbps)
3.8×10^{-3}	6.7%	85 Gbaud 16QAM	318	80 Gbaud 32QAM	375
1.25×10^{-2}	14.8%	100 Gbaud 16QAM	348	95 Gbaud 32QAM	413
2.4×10^{-2}	20%	90 Gbaud 32QAM	375	104 Gbaud 32QAM	433
5×10^{-2}	25%	104 Gbaud 32QAM	416	100 Gbaud 64QAM	480

In the subsequent sections, the single-polarization transmission experiment results are reported separately for each IQM. Then, we employ a DP emulator to determine the attainable transmission rate on a single optical carrier.

A. *Short IQM (Single Polarization)*

This section summarizes the transmission experiment results obtained using the short (3 mm) IQM. The IQM is reverse biased at 0.5 V, which corresponds to 30.5 GHz 3-dB bandwidth and minimizes the BER. For 80 km transmission, the optimum launch optical power (LOP) into the fiber is 3 to 4 dBm as illustrated in Fig. 5(e), which is limited by the fiber non-linearities. The BER performance after 80 km of SSMF is shown in Fig. 5(a) for different QAM orders. At line rates below 430 Gbps, 16QAM outperforms the other modulation formats because of its lower OSNR requirements. However, 32QAM performs better than 16QAM for the higher line rates due to the bandwidth limitations primarily from the SiP IQM and the RF amplifiers. Although the transmitter pre-emphasis filters pre-compensate the signal spectrum up to 64 GHz, the strong equalization after 50 GHz diminishes the AWG output signal swing; resulting in worse RF signal quality, smaller driving swing, higher modulation loss, and lower OSNR [17]. The summary of the achieved transmission rates is tabulated in Table I, considering different FEC thresholds. We considered 4 FEC thresholds based on the literature: (1) the 6.7% OH hard decision (HD) FEC with a BER threshold of 3.8×10^{-3}, (2) the 14.8% OH concatenated FEC (C-FEC) standardized for 400ZR with a BER threshold of 1.25×10^{-2} [18], (3) the 20% OH SD-FEC at a threshold BER of 2.4×10^{-2} [4], [6], and (4) the 25% OH SD-FEC with a BER threshold of 5×10^{-2} [9], [19]. Fig. 5(b) shows the OSNR performance of 16QAM and 32QAM at selected symbol rates after 80 km transmission. Compared to the theoretical OSNR performance and at the 2.4×10^{-2} SD-FEC threshold, the OSNR implementation penalty increases from 4 dB at 100 Gbaud 16QAM to 7.8 dB at 110 Gbaud 16QAM; a similar trend is observed for 32QAM. This increase in OSNR penalty with symbol rate is due to the lower ENOB of the AWG at higher symbol rates and the reduced signal fidelity with the stronger pre-emphasis, which adds more electrical noise from the transmitter side. Besides, the equalization-enhanced in-band

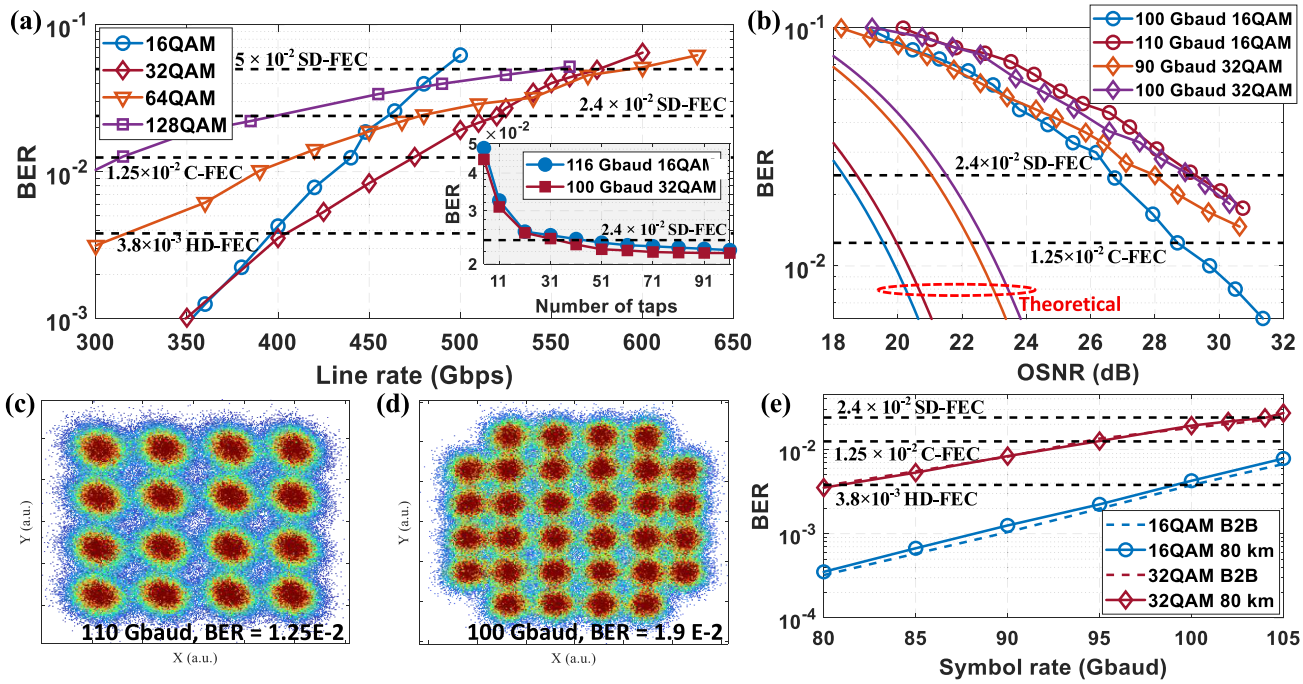

Fig. 6. (a) The achieved BER versus the line rate for different QAM orders after 80 km transmission using the long IQM. The inset shows BER sensitivity to the number of MIMO filter taps. (b) the OSNR performance at 0.1 nm resolution. The recovered constellations for (c) 110 Gbaud 16QAM and (d) 100 Gbaud 32QAM. (e) the BER versus symbol rate at B2B and after 80 km.

noise increases with symbol rate, which degrades the BER further at the same OSNR. However, the highest attained OSNR is limited by the modulation loss, which increases with the symbol rate because of the stronger pre-emphasis. Thus, we expect a higher OSNR implementation penalty and lower achievable OSNR with increasing the symbol rate. The processed constellations of 110 Gbaud 16QAM and 90 Gbaud 32QAM after 80 km of SSMF are shown in Fig. 5(c)–(d).

B. Long IQM (Single Polarization)

Likewise, the long (4 mm) modulator transmission results are presented in this section. The optimum reverse bias for minimum BER is 1V and corresponds to a 3-dB EO bandwidth of 25 GHz. The B2B results are presented in [20]. Fig. 6(a) shows the measured BER at different line rates for different formats after 80 km with the summary presented in Table I. Below the 6.7% OH HD-FEC BER threshold, QAM16 stands as the optimum modulation format. However, the transmission of 80 Gbaud 32QAM below the 6.7% OH HD-FEC BER threshold is achievable, corresponding to a line rate of 400 Gbps. The OSNR performance is given in Fig. 6(b), the maximum realized OSNR at 100 Gbaud 32QAM is 30.3 dB. At the 2.4×10^{-2} SD-FEC threshold, 100 Gbaud 16QAM exhibits an 8.5 dB OSNR implementation penalty compared to 10.5 dB at 110 Gbaud 16QAM. The inset of Fig. 6(a) shows the BER sensitivity of 116 Gbaud 16QAM and 100 Gbaud 32QAM after 80 km transmission to the number of employed equalizer taps. It is observed that 51 taps are sufficient for a BER below the 20% OH SD-FEC threshold; increasing the number of taps further improves the BER negligibly. Fig. 6(c)–(d) show the processed constellation of 110 Gbaud 16QAM and 100 Gbaud 32QAM, respectively. For

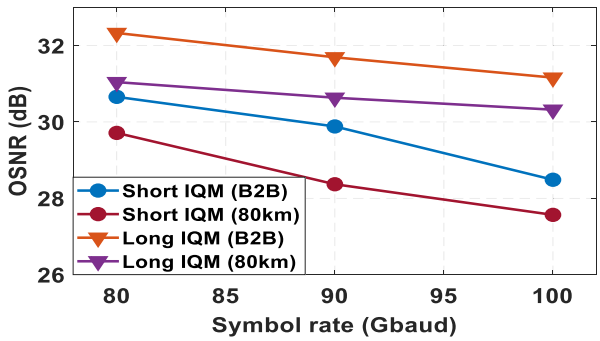

Fig. 7. The maximum achieved OSNR at 0.1 nm for 32QAM signals at different symbol rates.

32QAM, the outer constellation clusters experience more errors, which implies that non-linear pre-distortion of the transmitted symbols can improve the results considerably. The BER versus symbol rate at B2B and after 80 km for 16QAM and 32 QAM are depicted in Fig 6(e). The degradation of the BER due to the fiber transmission is negligible. Since the modulator is driven by only a fraction of the $2V_\pi$ swing, the optical extinction ratio is limited; leading to high modulation loss. Thus, the optical power just after the SiP chip is around -20 dBm due to the coupling and modulation loss. Therefore, the first EDFA is the dominant source of the noise in the system, and the noise added by the second EDFA leads to minor degradation in the BER performance.

Although the long IQM has lower bandwidth and induces a higher OSNR penalty compared to the short IQM, the long IQM yields better transmission performance. The higher OSNR

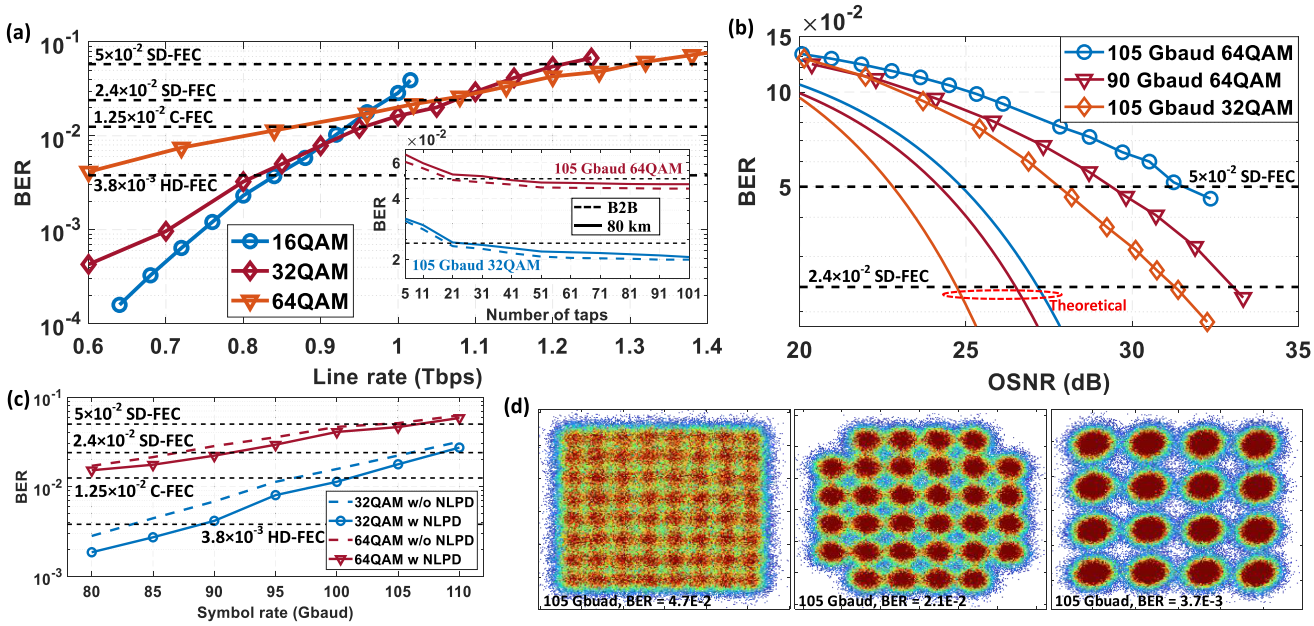

Fig. 8. (a) BER versus the line-rate for different QAM orders after 80 km, the inset shows the BER performances versus number of MIMO taps. (b) OSNR performance at 0.1 nm at B2B. (c) BER versus symbol rate with and without NLPD. (d) Received constellation of the X polarization for of 105 Gbaud 64QAM, 32QAM, and 16QAM after 80 km transmission.

penalty with the long IQM results from the higher equalization-enhanced noise because of its lower EO bandwidth. The employed RF amplifier has a slow roll-off frequency response up to 45 GHz and a saturation power of 20 dBm corresponding to 6 Vpp which is small compared to the IQMs V_π. Consequently, we experienced more limitations from the RF signal swing compared to the bandwidth limitations. This justifies the low reverse biases applied to both IQMs as the RF V_π increases with reverse bias voltage. Fig. 7 shows the measured OSNR as a function of symbol rate for 32QAM at B2B and after 80 km. The realized OSNR is approximately 2 dB higher for the long IQM; which results in better BER performance. We observe a $\sim$1 dB degradation in the OSNR after the 80 km transmission, which comes from the second EDFA noise. The higher OSNR in case of the long IQM is due to the higher modulation depth and lower modulation loss.

C. Long IQM (Dual Polarization)

Further, we employ DP emulation and non-linear pre-distortion (NLPD) of the transmitted symbols to improve the achieved performance using the long IQM. We retain the DSP routine presented in Fig. 4; however, we employ a 1D non-linear lookup table (NLLUT) for each quadrature with a 3-symbol memory length to pre-distort the generated symbols at the transmitter. The DP emulator used is composed of a polarization controller followed by a polarization beam splitter (PBS) to divide the power equally on both orthogonal polarizations. A variable optical delay line (VODL) is used to decorrelate both polarizations by inducing a delay of 9.2 ns for one polarization, which is equivalent to 920 symbols at 100 Gbaud. Then, the decorrelated orthogonal signals are combined by a polarization beam combiner (PBC) before transmission. The observed optimum launch optical power is 8 dBm, which is more than twice

TABLE II
SUMMARY OF NET BITRATE ACHIEVED AFTER 80 KM TRANSMISSION AND DP EMULATION

BER threshold	FEC OH	Modulation format	Net bitrate (Gbps)
3.8×10^{-3}	6.7%	105 Gbaud DP-16QAM	787
		80 Gbaud DP-32QAM	750
1.25×10^{-2}	14.8%	95 Gbaud DP-32QAM	827
		115 Gbaud DP-16QAM	800
2.4×10^{-2}	20%	105 Gbaud DP-32QAM	875
		85 Gbaud DP-64QAM	850
5×10^{-2}	25%	**105 Gbaud DP-64QAM**	**1008**
		115 Gbaud DP-32QAM	920

the value measured in the single polarization experiments as the transmitter-induced non-linearities are tackled by the NLPD. Aside from these 2 additions, the same experimental setup and DSP blocks are used, as shown in [10]. Fig. 8(a) shows the 80 km transmission results, where the reported BER is the average BER of both polarizations. We demonstrate the transmission of 105 Gbaud DP-64QAM below the 25% OH SD-FEC threshold, corresponding to a line rate of 1.26 Tbps and a net rate of 1 Tbps. The achieved performance at the different FEC thresholds is summarized in Table II. Fig. 8(b) depicts the OSNR performance at B2B, a 7 dB OSNR penalty is observed. The lower OSNR penalty compared to the single polarization results is coming from the BER improvement because of NLPD. At the highest measured OSNR, the BER noise floor is not reached, suggesting that better coupling and a higher driving signal swing can further improve the BER performance. Given the swing limitations, we operated the RF amplifiers beyond their 1 dB compression point, which degrades the linearity of the drive signal. Additionally, SiP IQMs have a non-linear transfer function that considerably

affects the higher QAM orders. Fig. 8(c) shows the BER versus symbol rate with and without NLPD for 32QAM and 64QAM. NLPD results in considerable BER improvement and reduces the OSNR implementation penalty, effectively improving the transmission performance. The inset of Fig. 8(a) shows the BER sensitivity to the MIMO filter length; 51 taps are adequate to reach the error floor similar to the single polarization results. Fig. 8(d) depicts the received constellation of the 105 Gbaud 16QAM, 32QAM, and 64QAM.

The power consumption of the SPP IQM excluding the TO heaters is given by $P = V_{rms}^2 / R$, where V_{rms} is calculated by integrating the Tx waveform, and R is the termination resistance [21]. Thus, the energy consumption per bit considering the transmission of 105 Gbaud 64QAM (Line rate of 630 Gbps) on a single polarization is 190 fJ/bit. The achieved transmission performance is mainly limited by the RF swing despite operating at twice the IQM electro-optic bandwidth. Thus, we needed to increase the clipping of signals beyond 100 Gbaud to limit their peak-to-average power ratio (PAPR) to a maximum of 10 dB. In this experiment, we relied on all-electronic equalization, which preserves the experimental architecture to that of conventional coherent transceivers and networks; however, it requires applying severe pre-emphasis for transmitting high symbol rates. Finally, we infer from our results that the new generation of AWGs and ASICs can enable a low bandwidth (25 GHz) SiP IQM to operate beyond 100 Gbaud and meet the 800G requirements, owing to the SiP IQM's slow roll-off frequency response.

V. Conclusion

This work presents the design and compares the transmission performance of two single-segment SiP C-band IQMs with 3 mm and 4 mm phase shifter lengths. The B2B and 80 km single-polarization transmission results along with the OSNR performance of both IQMs are reported. The long IQM outperforms the short one despite its inferior electro-optic bandwidth due to its higher phase-shifting efficiency (lower V_π). The OSNR measurements show that the long IQM exhibits a higher OSNR penalty; however, a higher OSNR is attainable compared to the short IQM, resulting in better BER performance. Using the long IQM, we transmit 95 Gbaud 32QAM over 80 km of SSMF at a BER below the 1.25×10^{-2} C-FEC threshold; corresponding to a net rate of 413 Gbps.

Using non-linear pre-distortion and dual-polarization emulation, we transmit 95 Gbaud DP-32QAM and 115 Gbaud DP-16QAM over 80 km under the 1.25×10^{-2} C-FEC threshold, which respectively represent net rates of 827 Gbps and 800 Gbps. Moreover, we demonstrate the transmission of 105 Gbaud DP-64QAM over 80 km below the 5×10^{-2} SD-FEC BER threshold using all-electronic equalization in a conventional coherent setup, featuring a record net rate of 1 Tbps. To the best of the authors' knowledge, the achieved transmission rates in this work are the highest reported at all the considered FEC thresholds using an all-silicon IQ modulator. Our results support single-segment SiP IQMs as a candidate technology for next-generation 800G coherent networks.

Acknowledgment

The authors would like to acknowledge CMC Microsystems for supporting the device fabrication.

References

[1] L. Wilkinson, "OIF launches 800G coherent and co-packaging framework IA projects, elects new board members/positions, officers and working group chairs," Dec. 2020. Accessed: Apr. 13, 2022. [Online]. Available: https://www.oiforum.com/technical-work/hot-topics/800g-coherent/

[2] S. Varughese, D. Lippiatt, S. Tibuleac, and S. E. Ralph, "Frequency dependent ENoB requirements for 400G/600G/800G optical links," *J. Lightw. Technol.*, vol. 38, no. 18, pp. 5008–5016, Sep. 2020.

[3] H. Sun et al., "800G DSP ASIC design using probabilistic shaping and digital sub-carrier multiplexing," *J. Lightw. Technol.*, vol. 38, no. 17, pp. 4744–4756, 2020.

[4] S. Zhalehpour et al., "All-silicon IQ modulator for 100 GBaud 32QAM transmissions," in *Proc. Opt. Fiber Commun. Conf.*, 2019, Paper. Th4A.5.

[5] S. Zhalehpour et al., "System optimization of an all-silicon IQ modulator: Achieving 100-Gbaud dual-polarization 32QAM," *J. Lightw. Technol.*, vol. 38, no. 2, pp. 256–264, Jan. 2020.

[6] S. Zhalehpour et al., "All silicon IQ modulator with 1Tb/s line rate," in *Proc. Opt. Fiber Commun. Conf. Exhibit.*, 2020, pp. 1–3.

[7] D. Patel, A. Samani, V. Veerasubramanian, S. Ghosh, and D. V. Plant, "Silicon photonic segmented modulator-based electro-optic DAC for 100 Gb/s PAM-4 generation," *IEEE Photon. Technol. Lett.*, vol. 27, no. 23, pp. 2433–2436, Dec. 2015.

[8] A. Samani et al., "Experimental parametric study of 128 Gb/s PAM-4 transmission system using a multi-electrode silicon photonic Mach Zehnder modulator," *Opt. Exp.*, vol. 25, no. 12, pp. 13252–13262, 2017.

[9] Z. Zheng et al., "Silicon IQ modulator for 120 Gbaud QAM," in *Proc. Eur. Conf. Opt. Commun.*, 2021, pp. 1–4.

[10] E. Berikaa, M. S. Alam, A. Samani, S. Lessard, and D. V. Plant, "Net 1 Tbps/λ transmission over 80 km of SSMF using a single segment SiP IQM with all-electronic equalization," in *Proc. Opt. Fiber Commun. Conf.*, 2022, Paper. Th4A.5.

[11] A. Samani et al., "A low-voltage 35-GHz silicon photonic modulator-enabled 112-Gb/s transmission system," *IEEE Photon. J.*, vol. 7, no. 3, 2015, Art. no. 7901413.

[12] A. Samani et al., "180 Gb/s single carrier single polarization 16-QAM transmission using an O-band silicon photonic IQM," *Opt. Exp.*, vol. 27, no. 10, pp. 14447–14456, 2019.

[13] D. Patel et al., "A 4 × 4 fully non-blocking switch on SOI based on interferometric thermo-optic phase shifters," in *Proc. Opt. Interconnects Conf.*, 2014, pp. 104–105.

[14] D. Petousi et al., "Monolithically integrated high-extinction-ratio MZM with a segmented driver in photonic BiCMOS," *IEEE Photon. Technol. Lett.*, vol. 28, no. 24, pp. 2866–2869, Dec. 2016.

[15] S. S. Azadeh et al., "Low V_π silicon photonics modulators with highly linear epitaxially grown phase shifters," *Opt. Exp.*, vol. 23, no. 18, pp. 23526–23550, 2015.

[16] M. Y. Sowailem et al., "770-Gb/s PDM-32QAM coherent transmission using InP dual polarization IQ modulator," *IEEE Photon. Technol. Lett.*, vol. 29, no. 5, pp. 442–445, Mar. 2017.

[17] B. M. Oliveira, A. Lorences-Riesgo, F. P. Guiomar, M. C. Medeiros, and P. P. Monteiro, "Optimizing probabilistic constellation shaping for amplifier-less coherent optical links," *J. Lightw. Technol.*, vol. 39, no. 13, pp. 4318–4330, Jul. 2021.

[18] E. Pincemin and Y. Loussouarn, "Silicon photonic ZR/ZR+ DCO-CFP2 interface for DCI and metro-regional 400G optical communications," in *Proc. Opt. Fiber Commun. Conf.*, 2021, pp. M3F.2.

[19] F. Buchali, A. Klekamp, L. Schmalen, and T. Drenski, "Implementation of 64QAM at 42.66 GBaud using 1.5 samples per symbol DAC and demonstration of up to 300 km fiber transmission," in *Proc. Opt. Fiber Commun. Conf.*, 2014, pp. M2A.1.

[20] E. Berikaa, M. S. Alam, A. Samani, S. Bernal, S. Lessard, and D. V. Plant, "Transmission of 100 GBaud 64QAM using an all-silicon IQ modulator," in *Proc. CLEO: Sci. Innovations*, 2022.

[21] D. Patel et al., "Design, analysis, and transmission system performance of a 41 GHz silicon photonic modulator," *Opt. Exp.*, vol. 23, no. 11, pp. 14263–14287, 2015.